Analysis of the time reversal operator for a scatterer undergoing small displacements

Franck D. Philippe, Claire Prada, and Mathias Fink
Institut Langevin, ESPCI, UMR CNRS 7587, 1 rue Jussieu 75231 Paris Cedex 05, France

Josselin Garnier
Laboratoire de Probabilités et Modèles Aléatoires & Laboratoire Jacques-Louis Lions, Université Paris Diderot, Site Chevaleret, Case 7012, Université Paris VII, 75205 Paris Cedex 05, France

Julien de Rosny[a]
Institut Langevin, ESPCI, UMR CNRS 7587, 1 rue Jussieu 75231 Paris Cedex 05, France

The method of the time reversal operator decomposition is usually employed to detect and characterize static targets using the invariants of the time reversal operator. This paper presents a theoretical and experimental investigation into the impact of small displacements of the target on these invariants. To find these invariants, the time reversal operator is built from the multistatic response matrix and then diagonalized. Two methods of recording the multistatic response matrix while the target is moving are studied: Acquisition either element by element or column by column. It is demonstrated that the target displacement generates new significant eigenvalues. Using a perturbation theory, the analytical expressions of the eigenvalues of the time-reversal operator for both acquisition methods are derived. We show that the distribution of the new eigenvalues strongly depends on these two methods. It is also found that for the column by column acquisition, the second eigenvector is simply linked to the scatterer displacements. At last, the implications on the Maximum Likelihood and Multiple Signal Classification detection are also discussed. The theoretical results are in good agreement with numerical and 3.4 MHz ultrasonic experiments.
© 2013 Acoustical Society of America. [http://dx.doi.org/10.1121/1.4768797]

I. INTRODUCTION

A time reversal mirror (TRM) provides a robust tool to focus a wave in space and time, whatever the complexity of the propagating medium. It has been applied in many different fields such as non-destructive testing,[1,2] medical therapy,[3–5] and underwater acoustics, either for detection[6,7] or for telecommunications.[8,9] A time reversal experiment is achieved in two steps: First, the TRM records the wave emitted by a source, and then these signals are flipped in time and emitted back into the medium. However, time-reversal invariance requires a stationary medium, thus the focusing of the time reversed signal is impaired when the medium is changed between the two steps. The effect of fluctuations on TRM performance has been quantitatively investigated in several papers.[10–12] For example, in underwater acoustics, Roux and Fink studied the degradation of the focal spot in a shallow water environment with waves on the surface, and Sabra and Dowling presented an analytical study of the effect of array deformation using modal decomposition and a statistical model.

This paper focuses on the DORT (French acronym for Decomposition of the Time Reversal Operator) method which is derived from the matrix formulation of iterative time-reversal experiments.[13] This method is an efficient way to detect and localize passive targets. In the frequency domain, the time reversal operator (TRO) is given by the Hermitian matrix $\mathbf{K}^{\dagger}\mathbf{K}$ (or $\mathbf{KK}^{\dagger}$) where $\mathbf{K}$ is the Multistatic Data Matrix (MDM) and the dagger superscript denotes transpose conjugation. For well-resolved isotropic scatterers, one eigenvector of the TRO, i.e., one time-reversal invariant, is generally associated with a single scatterer. Consequently, the rank of the TRO is equal to the number of scatterers. However, this property, which is important for detection, is only valid in a time-invariant environment. Indeed, previous studies assumed that the propagation medium and the targets were static during the acquisition of the MDM. But because the recording of the MDM is not instantaneous, this last assumption may not be realistic. This is especially true for at-sea experiments. For instance, in Prada *et al.*,[14] the DORT method was applied in shallow water using a 12 kHz vertical array composed of 24 transducers. Hence, 24 emissions and the 24 sound round-trip travels were necessary to acquire the MDM on the 24 transducer array. Thus it takes at least 8 s to detect targets at 250 m. As a consequence, instead of having 1 significant eigenvalue for detecting 1 target, the strongest eigenvalue is only 5 dB larger than a continuous distribution of the 23 other eigenvalues.

However, in this complex shallow water experiment, it is difficult to isolate the effects of the medium fluctuations from the effect of the ground reverberation that also increases the number of significant eigenvalues. Moreover, at sea, there are many possible causes of time fluctuations:

[a] Author to whom correspondence should be addressed. Electronic mail: julien.derosny@espci.fr

Array oscillations, gravity waves, non-stationary water currents, target motion, etc. Thus it is important to understand the effect of target motion on the time reversal invariants.

Because the general derivation of the invariants of the TRO is a tough problem, we consider a simple configuration for which analytical results can be derived: An isotropic point-like scatterer moving parallel to a linear array of transducers. Even in this simple case, it is observed that, instead of a unique time-reversal invariant for a motionless target, the scatterer is associated with as many invariants as the number of transducers. Here we study this effect when the displacements are small compared to the focal width at the target position. With this assumption, analytical results can be derived using Taylor expansions. It is very enlightening to understand the transition from a rank 1 TRO to a full rank TRO when the displacement range increases.

This paper is organized as follows. In Sec. II, the DORT method is briefly described and the two MDM acquisition methods are introduced. The theory describing the eigenvalue distribution is developed in Sec. III for column by column acquisition, and in Sec. IV for element by element acquisition. Both models are based on the Taylor expansion of the MDM with respect to the root-mean-square (rms) displacement of the target. Random matrix theory is used to describe the eigenvalue distribution for the element by element acquisition method. In addition, from the analysis of the eigenvectors of the TRO obtained with the column by column acquisition, we derive an original method to extract the target displacement which is even valid in the presence of phase aberration. In the last section we discuss how this approach can be applied to predict the resolution loss of two

well-known non-linear array processing algorithms: Minimum likelihood and multiple classification.

The theoretical results are confirmed with MDM obtained either numerically or experimentally. The experiments are performed with an ultrasonic transducer array working at 3.5 MHz central frequency.

II. EIGENVALUES OF THE TRO FOR A MOVING TARGET

A thorough description of the DORT method can be found in previous works[15,16] (and references therein), therefore only a few basic results are recalled in this section. For a given experiment with two arrays of transducers, two TROs can be introduced, the transmission operator (Tx-TRO) and the reception operator (Rx-TRO). They are, respectively, given by the matrix products $\mathbf{K}^\dagger \mathbf{K}$ and $\mathbf{K}\mathbf{K}^\dagger$. The Tx (respectively, Rx) time-reversal invariants are the eigenvalues, Σ_n^{Tx} (respectively, Σ_n^{Rx}) and the eigenvectors $\mathbf{U}_n^{Tx}$ (respectively, $\mathbf{U}_n^{Rx}$) of the Tx-TRO (respectively, Rx-TRO). It can be easily demonstrated that the nth eigenvalues of $\mathbf{K}^\dagger \mathbf{K}$ and $\mathbf{K}\mathbf{K}^\dagger$ are identical, i.e., $\Sigma_n^{Rx} = \Sigma_n^{Tx} = \Sigma_n$. Vector $\mathbf{U}_n^{Tx}$ (respectively, $\mathbf{U}_n^{Rx}$) is defined as the nth eigenvector of $\mathbf{K}^\dagger \mathbf{K}$ (respectively, $\mathbf{K}\mathbf{K}^\dagger$), i.e., $\mathbf{K}^\dagger \mathbf{K}\mathbf{U}_n^{Tx} = \Sigma_n \mathbf{U}_n^{Tx}$ (respectively, $\mathbf{K}\mathbf{K}^\dagger \mathbf{U}_n^{Rx} = \Sigma_n \mathbf{U}_n^{Rx}$). In the present study, a single array is used for transmission and reception, and acoustic reciprocity is assumed so that $\mathbf{K}$ is symmetrical and $\mathbf{K}\mathbf{K}^\dagger = \mathbf{K}\mathbf{K}^*$.

We consider an isotropic scatterer moving parallel to a linear array of transducers, slow enough to ignore the Doppler effects. In this configuration, we study two ways of acquiring the MDM. The first one, called "column by
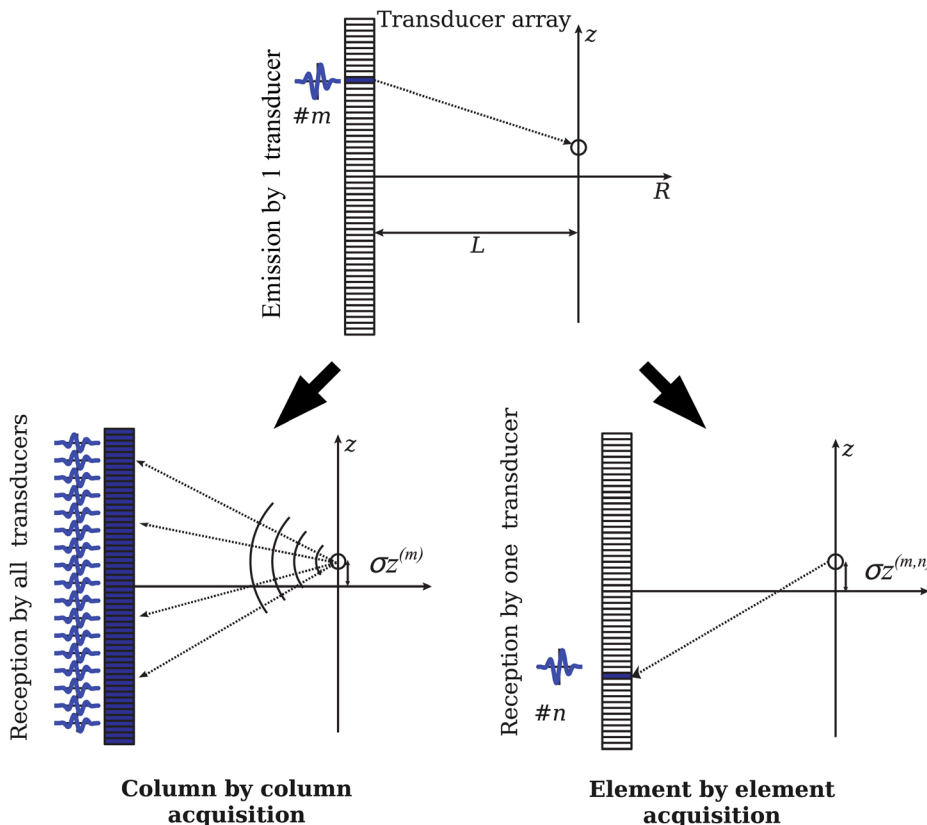

FIG. 1. (Color online) Experimental geometry and schematic description of the column by column and element by element acquisition methods.

J. Acoust. Soc. Am., Vol. 133, No. 1, January 2013

Philippe *et al.*: Time reversal and moving target   95

column," consists of successively transmitting a probing signal (pulse or chirp) from each of the transducers (Fig. 1). After each emission, the backscattered field is simultaneously recorded on all elements of the array. This method is commonly used in DORT experiments and the acquisition time is $2N\tau$, where N is the number of transducers in the array and τ is the one-way wave travel time between the array and the target. As the target moves between two emissions, each column of the acquired MDM corresponds to a different position of the target. The second one, which is used when there is no parallel processed reception, is the "element by element" acquisition. This method consists of N^2 Tx/Rx acquisitions, and the total acquisition time is $2N^2\tau$. It is therefore much more time consuming and, in this case, each element of $\mathbf{K}$ corresponds to a different scatterer's position.

To better understand the consequences of these two acquisition processes, simple numerical computations are performed to generate the TROs. The moving target, which is assumed to be isotropic and point-like, is set in the water at distance $L = 136$ mm from a 64-transducer linear array working at 3.5 MHz. The array pitch δ is 0.417 mm. The target motion is supposed to be parallel to the array. It is random following a zero-mean Gaussian distribution with a standard deviation denoted as σ. The N^2 elements K_{lm} of the MDM are computed as the product of the Green's function between antenna number l and the target's position, and the Green's function between the target and antenna number m. The synthetic Tx-TRO $\mathbf{K}^\dagger\mathbf{K}$ is then computed and diagonalized. Figure 2 displays the evolution of the eigenvalues of the Tx-TRO with respect to σ. Note that for a given σ, the plotted eigenvalues are obtained from one realization of the MDM. Hence, since the diagonalization is a self-averaging process there is no need for averaging. In these figures, in the static case ($\sigma = 0$), both acquisition methods give the same single positive eigenvalue. However, as σ increases, the eigenvalue distributions behave differently. For column by column acquisition, the eigenvalues increase roughly as a power law of σ [Fig. 2(b)]. For element by element acquisition, a continuous distribution of the eigenvalues rises. The distribution follows a quadratic law σ^2 for small σ. But the second eigen-

value separates from the continuum for $\sigma > 0.25$ mm and behaves like the second eigenvalue in the case of the column by column acquisition [Fig. 2(a)]. In both cases, the presence of secondary significant eigenvalues may induce false alarms as if more than one target is present in the medium. In order to identify these false alarms, the first step consists of solving the direct problem by predicting the evolution of the eigenvalues with respect to the target motion.

We propose two models associated with each acquisition method. The column by column results are explained thanks to Taylor's series of the TRO with respect to the rms displacement σ of the target. We show that the leading Taylor's order of the nth eigenvalue is $\sigma^{2(n-1)}$. To interpret the element by element results, we perform a Taylor's series of the TRO and also use fundamental results of random matrix theory (RMT) which predicts the eigenvalue distribution for a large random matrix. The whole analysis is performed in the frequency domain. For sake of simplicity, the frequency dependence is kept implicit.

III. ANALYSIS OF THE TRO FOR A COLUMN BY COLUMN ACQUISITION

The transfer matrix is acquired column by column by simultaneously recording the backscattered field on all array elements after each emission. This acquisition method is commonly used in experiments where a transmit-receive array is available, since it is much faster than the element by element acquisition.

A. Derivation of the TRO

Let us consider a linear array of aperture d with N transducers and a moving scatterer at a distance L from the array. Assuming a homogeneous and isotropic propagating media, K_{lm} is given by the propagation from transducer m at position M_m to the scatterer at position $S^{(m)}$ and the backscattering from the scatterer to the transducer at position M_l. Thus $K_{lm} = G(M_l, S^{(m)})G(S^{(m)}, M_m)$ where G is the Green's function. Using the free space Green's function,[17] it becomes
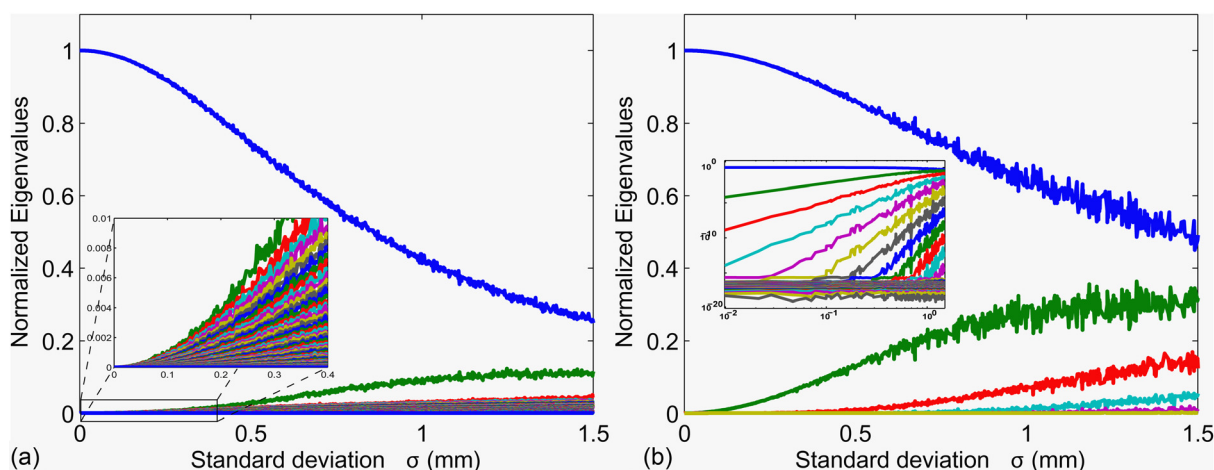

FIG. 2. (Color online) Evolutions of the 64 eigenvalues of the Tx-TRO at 3.5 MHz as a function of the rms displacement of the scatterer. (a) Element by element acquisition (the scatterer position is different for each MDM element). The inset plot is an enlargement between 0 and 0.4 mm. (b) Column by column acquisition. The scale of the inset plot is log-log.

$$K_{lm} = \frac{1}{16\pi^2 |M_l S^{(m)}||M_m S^{(m)}|} e^{ik(|M_l S^{(m)}|+|M_m S^{(m)}|)}, \quad (1)$$

where M_m $(1 \leq m \leq N)$ are the transducer positions.[18] Position $S^{(m)}$ does not depend on index l because a whole column is acquired for one scatterer position. Without loss of generality, the scattering coefficient is assumed equal to 1. Because in our configuration the target range is about 5 times the array size, the target can be considered far enough from the array to replace $1/|M_l S^{(m)}|$ and $1/|M_m S^{(m)}|$ by $1/L$. Then Eq. (1) becomes

$$K_{lm} = \frac{1}{16\pi^2 L^2} e^{ik(|M_l S^{(m)}|+|M_m S^{(m)}|)}. \quad (2)$$

Tx-TRO ($\mathbf{H} = \mathbf{K}^\dagger \mathbf{K}$) is then given by

$$H_{lm} = \frac{1}{(4\pi L)^4} e^{-ikM_l S^{(l)}} \left(\sum_n e^{ik(M_n S^{(m)}-M_n S^{(l)})} \right) e^{+ikM_m S^{(m)}}. \quad (3)$$

Matrix $\mathbf{H}$ is the product of two diagonal matrices and matrix $\tilde{\mathbf{H}}$. Indeed

$$H_{lm} = e^{-ikM_l S^{(l)}} \tilde{H}_{lm} e^{+ikM_m S^{(m)}}. \quad (4)$$

Because the diagonal matrices are unitary, $\mathbf{H}$ and $\tilde{\mathbf{H}}$ have the same eigenvalues and the lth component of the nth eigenvector of $\mathbf{H}$ is equal to the lth component of the nth eigenvector of $\tilde{\mathbf{H}}$ multiplied by $e^{-ikM_l S^{(l)}}$. For large N, the transformation of the discrete sum of Eq. (4) into a continuous one yields

$$\tilde{H}_{lm} = \frac{1}{(4\pi L)^4} \frac{N}{d} \int_{-d/2}^{d/2} e^{ik\left[\sqrt{L^2+(z-\sigma Z^{(m)})^2} - \sqrt{L^2+(z-\sigma Z^{(l)})^2}\right]} dz,$$
$$= F(\sigma Z^{(l)}, \sigma Z^{(m)}) \quad (5)$$

where $\sigma Z^{(l)}$ is the cross-range scatterer position for the lth emission (see Fig. 1). Distance σ is a displacement factor that is defined such as $\sum_{l=1}^{N} (Z^{(l)})^2 = N$. In the following, σ is assumed to be small compared to L, d, and $\sqrt{\lambda L/2\pi}$. Thus a Taylor expansion of the function F in terms of $\sigma Z^{(l)}$ and $\sigma Z^{(m)}$ can be performed. At the qth Taylor order, this series is written as

$$F(\sigma Z^{(l)}, \sigma Z^{(m)}) = \sum_{p,p'} \frac{\partial_{(p,p')} F(0,0)}{p! p'!} (\sigma Z^{(l)})^p (\sigma Z^{(m)})^{p'} + O(\sigma^{q+1}). \quad (6)$$

where $(p,p') \in [0,q]^2$, $(p+p') \leq q, (l,m) \in [1,N]^2$. In this equation, the TRO is expressed on a basis generated by $\{[Z^{(l)}]^n, n \in \mathbb{N}\}$; however, the sequences $\{Z^{(l)}, (Z^{(l)})^2, (Z^{(l)})^3, ..., (Z^{(l)})^n\}$ are not orthogonal (e.g., $\sum_l Z^{(l)}(Z^{(l)})^3 \neq 0$). Thus, to simplify the derivation, it is useful to write Eq. (6) on an orthonormal basis. The chosen basis $\{\tilde{\mathbf{V}}_m\}_{(1 \leq m \leq N)}$ is built from the well-known Gram-Schmidt orthonormalization of the family $\{[Z^{(l)}]^n, n \in \mathbb{N}\}$. The iterative procedure to derive $\tilde{\mathbf{V}}_m$ is described in Appendix A. Appendix A also provides the expressions of the first three vectors. By definition, one element of $\hat{\mathbf{H}}$ under this new basis is given by

$$\hat{H}_{(m+1)(m'+1)} = \tilde{\mathbf{V}}_m^\dagger \tilde{\mathbf{H}} \tilde{\mathbf{V}}_{m'}. \quad (7)$$

Note that the dimension of $\hat{\mathbf{H}}$ is infinite. But, thanks to this orthonormalization, the elements of the matrix are sorted with respect to their Taylor's order. More precisely, the Taylor order of each element of an anti-diagonal is given by the number of elements of the anti-diagonal minus 1. For instance, the Taylor's fifth order expansion is given by

$$\quad (8)$$

The method to compute the matrix elements up to order 2 is described in Appendix B. This method can be generalized to compute them up to an arbitrary order. The use of a symbolic algebra software makes the task much easier to achieve.

Therefore, computation of the eigenvalues and the eigenvectors up to the kth Taylor order means the diagonalization of the upper-left sub-matrix of dimensions $(k+1, k+1)$.

B. Eigenvalues

In this section the displacement distribution is assumed symmetrical with respect to the array axis. We show in Appendix C that in such a case, the element $\hat{H}_{mm'}$ equals zero when indexes m and m' are of different parities. Consequently Eq. (8) becomes

The expressions of the matrix elements are given in Appendix D. Matrix $\hat{\mathbf{H}}$ can be decomposed into two independent matrices: The first one is built from $\hat{H}_{2n,2n'}$ elements and the other from $\hat{H}_{2n+1,2n'+1}$ elements. Hence the diagonalizations of both sub-matrices provide the eigenvalues of $\hat{\mathbf{H}}$. Even with these simplifications, the extraction of the

TABLE I. Fourth order Taylor expansion of the eigenvalues of $\hat{\mathbf{H}}$.

Taylor order	Eigenvalues Σ_n
1	$N^2 + \sigma^2(-d^2N^2k^2/12L^2) + \sigma^4(d^2N^2k^2/4L^4 + 7d^4N^2k^4 + 720L^4)$
2	$\sigma^2(d^2N^2k^2 + 12L^2) + \sigma^4(d^4N^2k^4 + 80L^4 - d^2N^2k^2 + 4L^4)$
3	$\sigma^4(d^4N^2k^4 + 360L^4)$

eigenvalues is quite laborious. The expansions of the first three eigenvalues Σ_1, Σ_2, and Σ_3 up to the fourth order are given in Table I.

Up to order σ^2, these expressions of the eigenvalues only require that $\sum_l Z^{(l)} = 0$ (there is no statistical assumption on $Z^{(l)}$). But at higher order, they are based on the law of large numbers and the displacements are assumed random with a Gaussian distribution. Within these two assumptions, σ as defined after Eq. (5) is also the standard deviation of the target motion. The eigenvalues shown in Table I are obtained using a computer algebra software (MUPAD) and by performing the diagonalization of a 3×3 matrix and a 2×2 matrix. The derivation of the general case is beyond the scope of this paper.

These analytical results are compared to eigenvalues deduced from synthetic TRO [Fig. 3(a)] and from experimental TRO [Fig. 3(b)]. The data are measured with a 64-transducer array working at $3.4\,\text{MHz}$ ($\lambda = 0.43\,\text{mm}$). The array pitch is $\delta = 0.417\,\text{mm}$ so that the array aperture is equal to 26.7 mm. The target is a 0.1 mm diameter steel wire placed at $L = 136\,\text{mm}$. A stepping motor translation stage moves the target following a programmed pseudo random (zero mean Gaussian distributed) displacement sequence.

As can be seen in Fig. 3, the model successfully predicts the evolution of the eigenvalues of the TRO as a function of σ when this last is smaller than 0.3 mm.

C. Eigenvectors

After a careful study of the eigenvalues, we now focus on the eigenvectors and their numerical back-propagation (i.e., beamforming). The Rx and Tx back-propagated fields

of the qth eigenvector at position $P = (L, z)$ are expressed as $|\sum_l \exp(-ikM_lP)[\mathbf{U}_q^{Rx}]_l|$ and $|\sum_l \exp(+ikM_lP)[\mathbf{U}_q^{Tx}]_l|$. In Figs. 4(a) and 4(b), these back-propagated fields are plotted at range L and on z-axis for the first four Tx and Rx eigenvectors computed for $\sigma = 0.54\,\text{mm}$. We first note that $\mathbf{U}_1^{Rx}$ and $\mathbf{U}_1^{Tx}$ are close to the eigenvectors in the motionless case ($[\mathbf{U}_1^{Tx}]_l \approx e^{ik|M_lS^{(l)}|}/\sqrt{N}$). Consequently, they are focused at the average target location. Second, we see that $\mathbf{U}_q^{Tx}$ is no longer equal to $(\mathbf{U}_q^{Rx})^*$ when $q > 1$, as it should be if the experiment was static. This is due to the symmetry breaking of $\mathbf{K}$ matrix for $\sigma > 0$. Indeed, the target position is now different for each column. In Figs. 4(c) and 4(d), the experimental results show the same behavior, even if the mean target position is not exactly centered with the transducer array.

Matrix $\hat{\mathbf{H}}$ is not diagonal, i.e., the vectors $\tilde{\mathbf{V}}_m$ are not the eigenvectors of $\tilde{\mathbf{H}}$. But since the off-diagonal elements are small compared to the diagonal elements, $\tilde{\mathbf{V}}_m$ are good approximations of the mth eigenvectors at zero order.

Hence, the leading term of the second eigenvector of $\hat{\mathbf{H}}$ is $\tilde{\mathbf{V}}_1 = \{Z^{(l)}/\sqrt{N}\}_{1 \leq l \leq N}$. Using Eq. (4), the second eigenvector of $\mathbf{H} = \mathbf{K}^\dagger\mathbf{K}$ is then approximated by

$$[\mathbf{U}_2^{Tx}]_l \approx \frac{e^{ik|M_lS^{(l)}|}Z^{(l)}}{\sqrt{N}}. \tag{9}$$

Note that the indexes of the eigenvectors of $\hat{\mathbf{H}}$ start at 0 while the ones of $\mathbf{H}$ start at 1. This difference comes from the fact that $\tilde{\mathbf{V}}_n$ is derived from a Taylor expansion while $\mathbf{U}_m^{Tx}$ is an experimental observable. The ratio of the lth element of $\mathbf{U}_2^{Tx}$ by the lth of element of $\mathbf{U}_1^{Tx}$ which is equal to $e^{ik|M_lS^{(l)}|}/\sqrt{N}$ leads to the target position $Z^{(l)}$ during the acquisition of the lth column of the MDM. The absolute displacement of the target is $\sigma Z^{(l)}$ and σ is obtained from the ratio of the two first eigenvalues. Finally it becomes

$$\sigma Z^{(l)} = \sqrt{\frac{\Sigma_2}{\Sigma_1}} \frac{2\sqrt{3}L}{kd} \frac{(\mathbf{U}_2^{Tx})_l}{(\mathbf{U}_1^{Tx})_l}. \tag{10}$$

We recall that Σ_1 and Σ_2 are the first and second eigenvalues, L is the target range, and d is the array width.
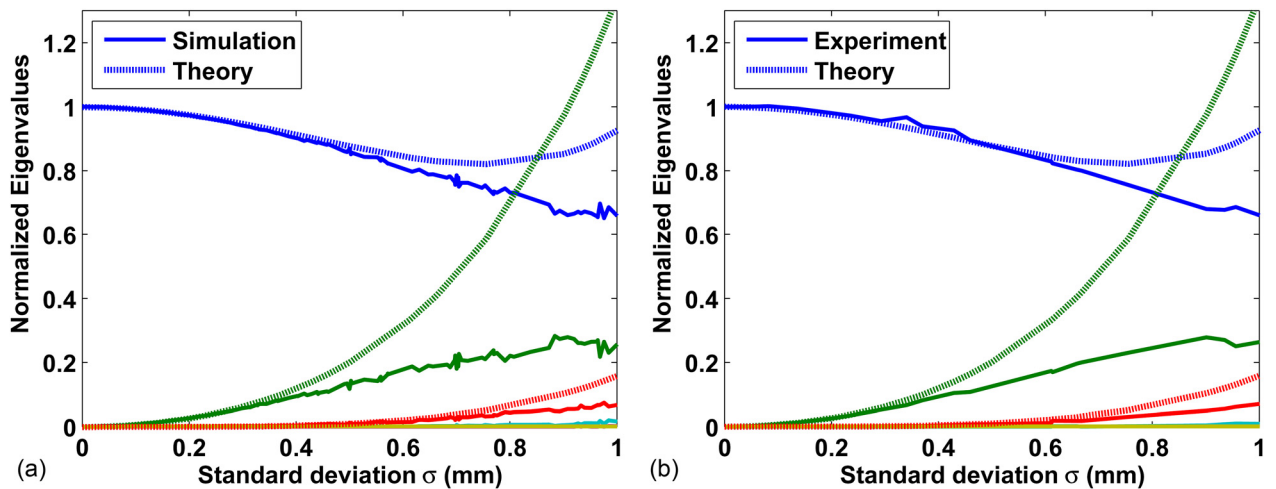

FIG. 3. (Color online) Eigenvalues (solid line) of synthetic TRO (a) and of the experimental TRO (b) as a function of σ for the column by column acquisition. The results are compared to the analytic expressions obtained with a second order Taylor expansion (dashed lines).
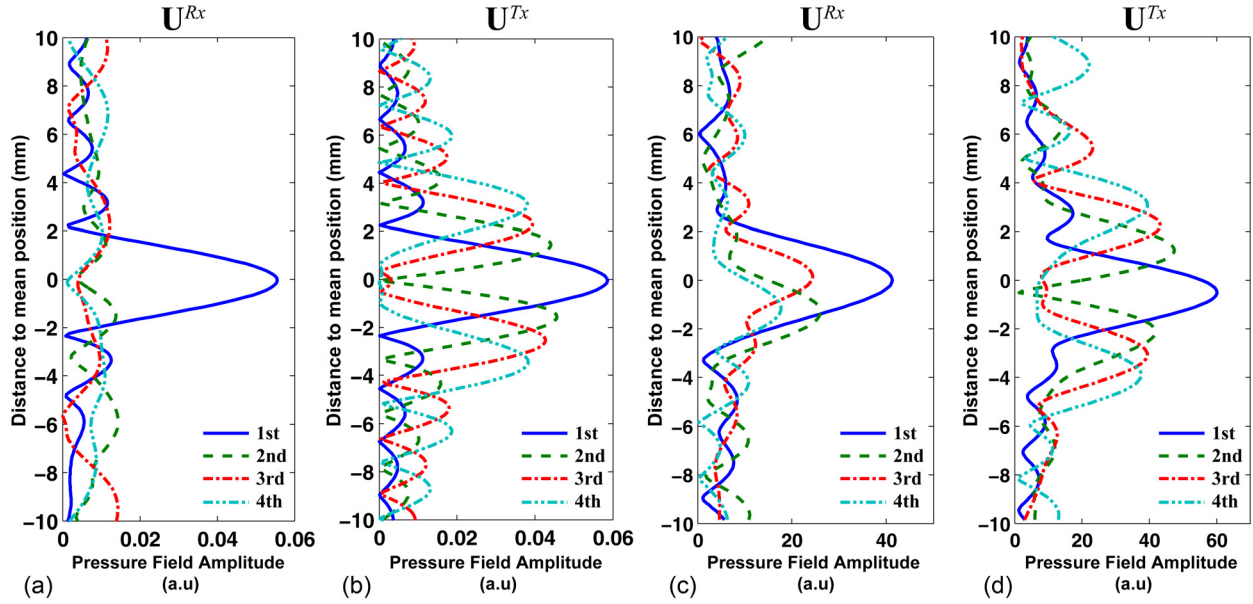
FIG. 4. (Color online) Back-propagation (or beamforming) of the first four eigenvectors on the z-axis at range L for column by column acquisition with $\sigma = 0.54$ mm. The eigenvectors $\mathbf{U}_q^{Tx}$ used for (a) and $\mathbf{U}_q^{Rx}$ used for (b) are deduced from synthetic TRO. The eigenvectors $\mathbf{U}_q^{Tx}$ used for (c) and $\mathbf{U}_q^{Rx}$ used for (d) are deduced from the experimental data.

Experimental results plotted in Figs. 5 and 6 are obtained with a random displacement and a linearly accelerated target. In both cases, there is an excellent agreement between the positions deduced from Eq. (10) and the real ones.

As can be seen in Figs. 5(a) and 6(a), for small values of σ the use of Eq. (10) provides an original way to track a target. This method differs from the match-filter based techniques proposed in underwater acoustics[19–21] as the displacements of the targets are directly deduced from the absolute value of $\mathbf{U}_2^{Tx}$.

However as σ increases, the zero order Taylor expansions of $\mathbf{U}_1^{Tx}$ and $\mathbf{U}_2^{Tx}$ are not sufficiently accurate, so it becomes difficult to compensate for the phase term of $\mathbf{U}_2^{Tx}$ [Figs. 5(b) and 6(b)]. This is striking for $\sigma > 0.6$ mm, where the third eigenvalue begins to stand out from the noise [see Fig. 3(a)]. In order to give a quantitative measurement of the mismatch between derived and real positions, the deviation induced by the error made on the position derived by Eq. (10) is compared to $\hat{H}_{42}/\hat{H}_{22}$. Indeed, by using the zero order approximation of $\mathbf{U}_2^{Tx}$, de facto, the term $\hat{H}_{42}$ is neglected. It stands to reason that the ratio $\hat{H}_{42}/\hat{H}_{22}$ will give an estimation of the error. This approach is confirmed in Fig. 7 where this quantity is compared to the error made on the derived positions. In this figure, the standard deviation of the error clearly follows the coupling term, proving their relation. Thanks to $\hat{H}_{42}/\hat{H}_{22}$ we deduce a validity criterion for Eq. (10) related to the well-known resolution quantity $\lambda L/d$. Indeed, $\hat{H}_{42}/\hat{H}_{22} < 0.1$ when $\sigma < 0.06\lambda L/d$, only then the tracking of the target can be trusted.

This tracking technique offers one more advantage compared to matched-filter based methods. Indeed, going back to Eq. (4), we conclude that this method is working even when phase aberrations occur in front of the array. If the aberrator induces a phase shift φ_n at the nth transducer of the array

then the new MDM becomes $\mathbf{K}_{ab} = \mathbf{PKP}^*$ where the diagonal matrix $\mathbf{P}$ represents the aberration effect $(P_{n,n} = e^{i\varphi_n})$. The (l,m) element of Tx-TRO $(\mathbf{H}_{ab} = \mathbf{K}_{ab}^\dagger \mathbf{K}_{ab})$ with the aberrator is expressed as

$$(\mathbf{H}_{ab})_{lm} = \sum_k^N e^{-i\phi_l} K_{lk}^* e^{-i\phi_k} e^{+i\phi_k} K_{km} e^{+i\phi_m}.$$

$$(\mathbf{H}_{ab})_{lm} = e^{-i\phi_l} \sum_k^N K_{lk}^* K_{km} e^{+i\phi_m} = e^{-i\phi_l} H_{lm} e^{+i\phi_m}. \tag{11}$$
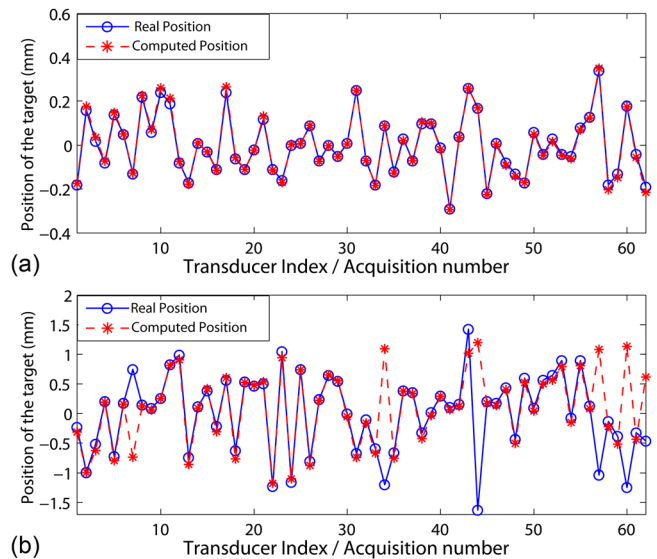

FIG. 5. (Color online) Experimental estimation of the random motion of the target. Comparison between the real positions of the target (−o) and the position deduced from the DORT analysis [see Eq. (10)] (−*). (a) is obtained for $\sigma = 0.14$ mm and (b) for $\sigma = 0.66$ mm.
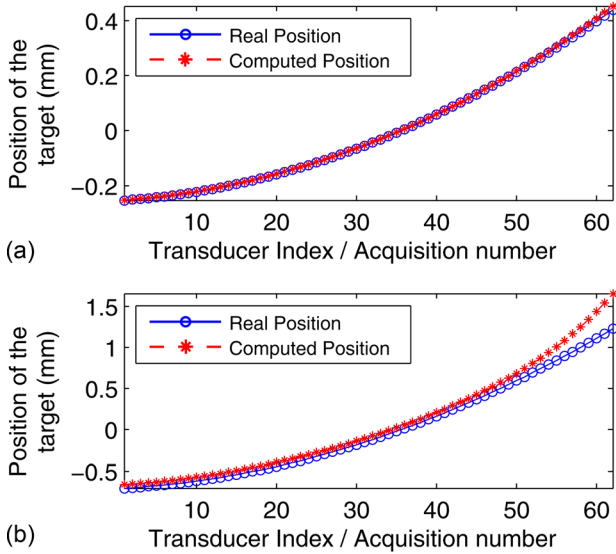
FIG. 6. (Color online) Case of a linear, accelerated motion of the target. Comparison between the real positions of the target ($-o$) and the position deduced from DORT analysis [see Eq. (9)] ($-*$). (a) is obtained for $\sigma = 0.14$ mm and (b) is obtained for $\sigma = 0.66$ mm. The TRO is computed from synthetic data.

This equation is similar to Eq. (4), when doing the same derivation, the target displacement is also given by Eq. (10), i.e., it is proportional to the ratio of the elements of the two first eigenvectors.

With a strong random phase aberrator in front of the transducer array, we compute the synthetic TRO. We compare the localization using Eq. (10) to the classical beam forming. We note that when no noise is added [Fig. 8(a)], both approaches provide very good estimations of the target positions. Indeed, although the beamformed map looks like a speckle pattern due to the unknown phase aberrator (there is no focal spot at the target position), for small target displacements, the speckle pattern is shifted proportionally. But when strong noise is added, we observe in Fig. 8(b), contrary to the DORT approach, beamforming does not work anymore. Thus DORT appears to be more robust to noise.
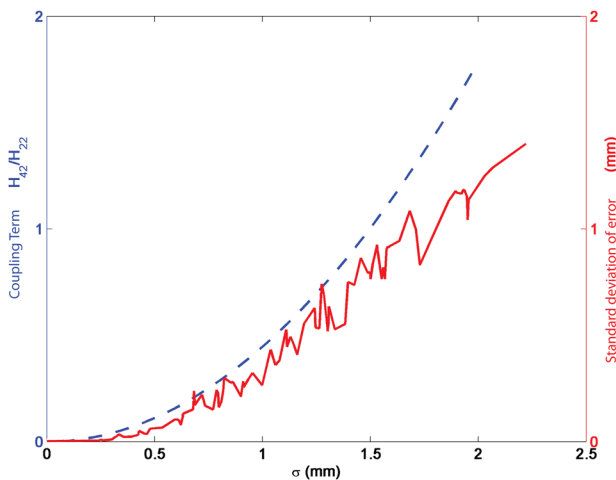

FIG. 7. (Color online) Error made on the position deduced from Eq. (10) (solid line) compared to $\hat{H}_{42}/\hat{H}_{22}$ (dashed line).

IV. ANALYSIS OF THE TRO FOR AN ELEMENT BY ELEMENT ACQUISITION

A. Eigenvalues

The Cartesian coordinates of the target position $S^{(lm)}$ during acquisition of the K_{lm} element is $(L, 0, \sigma Z^{(lm)})$ where $Z^{(lm)}$ is a normal random variable with zero mean and unitary variance. Contrary to the column by column acquisition, the position of the scatterer is different (uncorrelated) for each element of the matrix **K**.

Using the Green's function in free space, the elements of the MDM are written as

$$K_{lm} = \frac{1}{16\pi^2 |M_l S^{(lm)}||M_m S^{(lm)}|} e^{ik(|M_l S^{(lm)}| + |M_m S^{(lm)}|)}, \quad (12)$$

with $k = \omega/c$ the intrinsic wavenumber.

Considering that $L \gg d \gg \sigma$, K_{lm} simplifies to

$$K_{lm} = \frac{1}{16\pi^2 L^2} e^{ik\sqrt{L^2 + z_l^2}} e^{ik\sqrt{L^2 + z_m^2}}$$
$$\times e^{-ik\sigma(z_l Z^{(lm)}/\sqrt{L^2 + z_l^2} + z_m Z^{(lm)}/\sqrt{L^2 + z_m^2})}, \quad (13)$$

where z_l is the transversal position of the first transducer of the array. In addition, we also consider the case where N is large enough to apply the law of large numbers.

One can show that the rank of the first order Taylor expansion of **K** is equal to N. This is a major difference with the column by column case where this rank equals 1. Consequently, RMT should be applied to interpret the element by element MDM. To this end, we distinguish the mean value of the MDM from its fluctuating part: $K_{lm} = \langle K_{lm} \rangle + \delta K_{lm}$.

The analysis of the eigenvalue distribution of the matrix $\mathbf{K}^\dagger \mathbf{K}$, where **K** can be described as a deterministic matrix $\langle \mathbf{K} \rangle$ perturbed by a random matrix $\delta \mathbf{K}$ has recently attracted
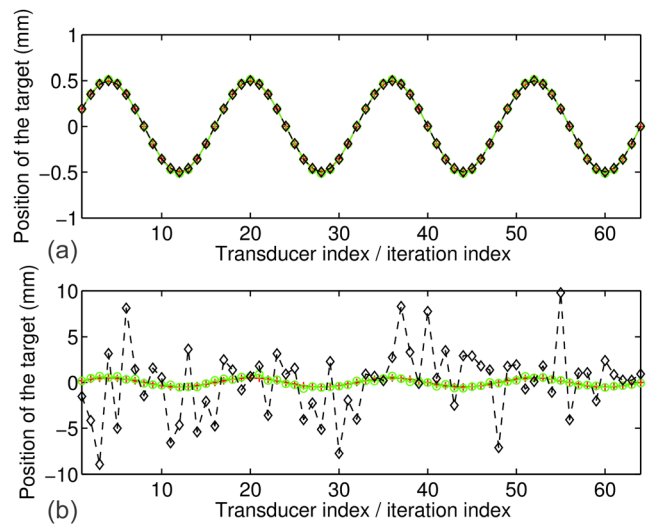

FIG. 8. (Color online) Displacement of a target with respect to the iteration index when a strong and random phase aberrator is in front of the array. The solid line with plus markers is the exact position of the scatterer, solid line with circle markers is deduced from Eq. (10), and the dotted line with diamonds is the position extracted from the displacements of the maximum of the beamformed map. (a) No noise is added to the MDM. (b) Decorrelated Gaussian noise is added to each element of the MDM with a SNR equal to 1.

attention, and we will use some of the results reported in the literature.[22–24] In the following we will first show that the mean value of the matrix $\mathbf{K}$ is indeed a low-rank matrix and compute its eigenvalues, and then we will show how the eigenvalue distribution is affected by the addition of random fluctuations.

The mean value of $\mathbf{K}$, written as $\langle \mathbf{K} \rangle$, is given by

$$\langle K_{lm} \rangle = \frac{1}{(4\pi L)^2} e^{ik\sqrt{L^2+z_{lm}^2}} e^{ik\sqrt{L^2+z_{lm}^2}}$$
$$\times \int dx \frac{e^{-x^2/2}}{\sqrt{2\pi}} e^{-ik\sigma(z_l/\sqrt{L^2+z_l^2}+z_m/\sqrt{L^2+z_m^2})x}. \quad (14)$$

Assuming z_l and z_m are small compared to L, it becomes

$$\langle K_{lm} \rangle \simeq \frac{1}{(4\pi L)^2} e^{ik\sqrt{L^2+z_l^2}} e^{ik\sqrt{L^2+z_m^2}} e^{(-k^2\sigma^2/2L^2)(z_l+z_m)^2}. \quad (15)$$

The distributions of the eigenvalues of $\langle \mathbf{K}^\dagger \rangle \langle \mathbf{K} \rangle$ given by Eqs. (13) and (15) are compared in Fig. 9. The eigenvalues of the mean matrix successfully describes the evolution of the two first eigenvalues of $\mathbf{K}^\dagger \mathbf{K}$ obtained without averaging.

Next, to find the analytical expression of these two first eigenvalues, we use the same approach as for the column by column case. A Taylor expansion of $\langle \mathbf{K} \rangle$ up to the fourth order is derived,

$$\langle K_{lm} \rangle = \frac{1}{(4\pi L)^2}$$
$$\times e^{ik\sqrt{L^2+z_l^2}} \left[1 - \frac{k^2\sigma^2(z_l+z_m)^2}{2L^2} + \frac{k^4\sigma^4(z_l+z_m)^4}{8L^4} \right]$$
$$\times e^{ik\sqrt{L^2+z_m^2}} + O(\sigma^6). \quad (16)$$

To compute the eigenvalues, Eq. (16) is projected onto a new orthonormal basis built from Gram-Schmidt orthonormalization. This part is similar to what has been done in Sec. III A but instead of using the positions of the target from the generating family, we use the positions of the transmit/receive elements ($\{1, z_i, z_i^2, \ldots\}$). After some derivations, the two first eigenvalues of $\langle \mathbf{K}^\dagger \rangle \langle \mathbf{K} \rangle$ are as follows:

$$\Sigma_1 \simeq \frac{N^2}{(4\pi L)^4} \left[1 - \frac{k^2\sigma^2 d^2}{12L^2} + \frac{7k^4\sigma^4 d^4}{720L^4} \right]^2,$$
$$\Sigma_2 \simeq \frac{N^2}{(4\pi L)^4} \left[\frac{k^2\sigma^2 d^2}{12L^2} - \frac{k^4\sigma^4 d^4}{80L^4} \right]^2. \quad (17)$$

Here, it is assumed that N is large. As shown in Fig. 9, the analytical expression of the first eigenvalue up to order 4 is in good agreement with the simulated eigenvalues for $\sigma < 0.6$ mm. As for Σ_2, it is primarily below the second eigenvalue due to the fluctuating part of $\mathbf{K}$. Then it increases rapidly but the Taylor expansion is no longer valid.

Thus we have shown that the first two eigenvalues of $\mathbf{K}^\dagger \mathbf{K}$ observed in Fig. 9 are mostly due to $\langle \mathbf{K}^\dagger \rangle \langle \mathbf{K} \rangle$. Next we
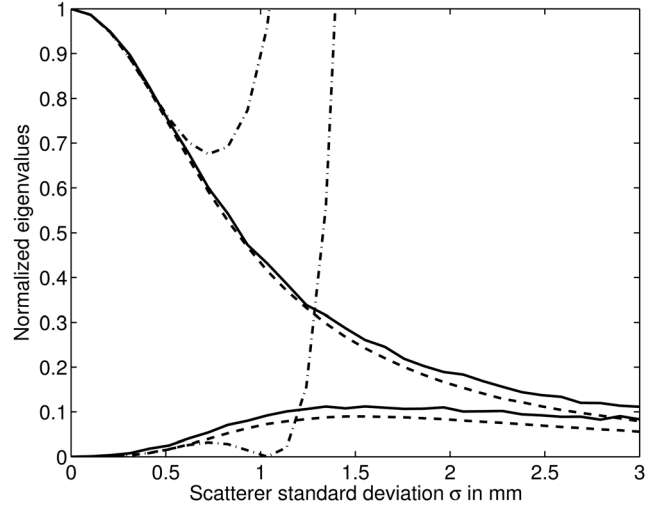

FIG. 9. First two eigenvalues of $\mathbf{K}^\dagger \mathbf{K}$ as a function of σ for the element by element acquisition (continuous lines). For each element of K, the position of the scatterer is different. Here $\mathbf{K}$ is a synthetic MDM, i.e., it has been numerically computed from the Green's function (see Sec. II for more details). These eigenvalues are compared to those of $\langle \mathbf{K}^\dagger \rangle \langle \mathbf{K} \rangle$ (dashed line). An element $\langle K_{lm} \rangle$ is estimated numerically by averaging K_{lm} over 100 different positions. The dashed–dotted lines correspond to the Taylor expansions of the first and second eigenvalues [Eq. (17)].

show that the other eigenvalues (for clarity they are not shown in Fig. 9) are mainly originated from the fluctuating part $\delta \mathbf{K}$. They are deduced from the variance of element K_{lm}. For small σ, it is given by

$$\langle K_{lm}^2 \rangle - \langle K_{lm} \rangle^2 = \frac{k^2\sigma^2}{256\pi^4 L^4} \left(\frac{z_l}{\sqrt{L^2+z_l^2}} + \frac{z_m}{\sqrt{L^2+z_m^2}} \right)^2. \quad (18)$$

The result clearly depends on both entries l and m. In general, there is no analytical formulation in the case of a random matrix with element variance dependent on the two element indexes. Nevertheless, we assume that the statistical properties of the fluctuating part of $\mathbf{K}$ mainly depend on the variance averaged over all the elements of $\mathbf{K}$. From Eq. (18) the average value over the matrix index is

$$\frac{1}{N^2} \sum_{lm} \langle K_{lm}^2 \rangle - \langle K_{lm} \rangle^2$$
$$= \frac{k^2\sigma^2}{256\pi^4 L^4 N^2} \sum_{lm} \left(\frac{z_l^2}{L^2+z_l^2} + \frac{2z_l z_m}{\sqrt{L^2+z_l^2}\sqrt{L^2+z_m^2}} + \frac{z_m^2}{L^2+z_m^2} \right). \quad (19)$$

The second term on the right-hand side vanishes because the array is symmetrical with respect to $z = 0$ axis. The first and the third terms are equal to $(N^2/d) \int_{-d/2}^{d/2} z_l^2/(L^2 + z_l^2) dz_l$. The continuous integral replaces the discrete sum. Hence, the averaged variance is equal to $k^2\sigma^2/128\pi^4 L^4 \left(1 - (2L/d)\arctan(d/2L) \right)$.

The spectral properties of a uniform random matrix are well known. In particular, it has been shown[25] that, for large

J. Acoust. Soc. Am., Vol. 133, No. 1, January 2013

Philippe *et al.*: Time reversal and moving target   101

matrices, there is a deterministic maximum to the singular value distribution.[26] Hence, the maximum eigenvalue (the square of the maximum singular value) is given by

$$\Sigma_{\text{var}} = 8N(k\sigma/16\pi^2L^2)^2\left(1 - 2L/d \arctan(d/2L)\right).$$
(20)

Assuming $d \ll 2L$, Eq. (20) can be simplified to

$$\frac{\Sigma_{\text{var}}}{\Sigma_1} = \frac{2}{3N}\left(\frac{dk\sigma}{L}\right)^2.$$
(21)

In Figs. 10(a) and 10(b), we observe that, for small σ, Eq. (21) approximately fits the eigenvalues of both synthetic and experimental TRO.

B. Eigenvectors

The phase and the amplitude of the three first transmission eigenvectors measured at $\sigma = 0.70$ mm are plotted in Fig. 11(a). As expected, the two first eigenvectors are given by the diagonalization of the mean matrix $\langle \mathbf{K}^\dagger \rangle \langle \mathbf{K} \rangle$, i.e., $[\mathbf{U}_1^{Tx}]_l \approx e^{ik\sqrt{L^2+z_l^2}}/\sqrt{N}$ and $[\mathbf{U}_2^{Tx}]_l \approx z^{(l)}e^{ik\sqrt{L^2+z_l^2}}/\sqrt{N}$, respectively. As for the third eigenvector, it is due to the fluctuating part of the matrix and, consequently, the phase and amplitude of each component are random. Figure 11(b) shows that one may use the two first eigenvectors to find the mean position of the target but unlike the column by column case, the information on the positions of the target is, to the authors' knowledge, not extractable. It is worth noting that the first eigenvector corresponds to a monopolar focus while the second eigenvector corresponds to a dipolar focus, even when the target in itself is an isotropic scatterer. Thus the mean value of MDM is the MDM of a sort of average extended target. Indeed, in such a case, we have already shown that beamforming of the first and second eigenvector gives rise to such patterns.

V. DISCUSSION ON THE IMPACT ON MUSIC AND ML DETECTION

Up to now, we have only focused on the analysis of the invariants of the TRO and their back-propagation. In 2003, Prada and Thomas[27] showed that two classical detection algorithms, Maximum Likelihood (ML) and MUltiple SIgnal Classification (MUSIC) can be introduced within the framework of DORT. The ML and MUSIC expressions in terms of time-reversal invariants are given by

$$I_{\text{ML}}^{Tx,Rx}(P) = \left(\sum_{q=1}^{N}\Sigma_q^{-1}\left|\sum_{l=1}^{N}\exp\left(\pm ik\sqrt{L^2+z_l^2}\right)[\mathbf{U}_q^{Tx,Rx}]_l\right|^2\right)^{-1},$$
(22)

$$I_{\text{MUSIC}}^{Tx,Rx}(P) = \left(\sum_{q=2}^{N}\left|\sum_{l=1}^{N}\exp\left(\pm ik\sqrt{L^2+z_l^2}\right)[\mathbf{U}_q^{Tx,Rx}]_l\right|^2\right)^{-1}.$$
(23)

We compare these two non-linear estimators to the robust beam forming estimator

$$I_{BF}^{Tx,Rx}(P) = \sum_{q=2}^{N}\Sigma_q\left|\sum_{l=1}^{N}\exp(\pm ik\sqrt{L^2+z_l^2})[\mathbf{U}_q^{Tx,Rx}]_l\right|^2.$$
(24)

Because the target is moving during acquisition of the MDM, the three estimators are affected and can provide different results when using the Tx or Rx eigenvectors. Note that + (respectively, −) sign in Eqs. (22)–(24) are related to Tx (respectively, Rx) eigenvectors. These estimators computed from synthetic MDM are plotted in Fig. 12. For a motionless target [Fig. 12(a)], as expected, the localization is excellent with both ML and MUSIC estimators. The sharpness of the spot is only limited by the 60 dB signal-to-noise ratio (SNR). But when the target moves during MDM
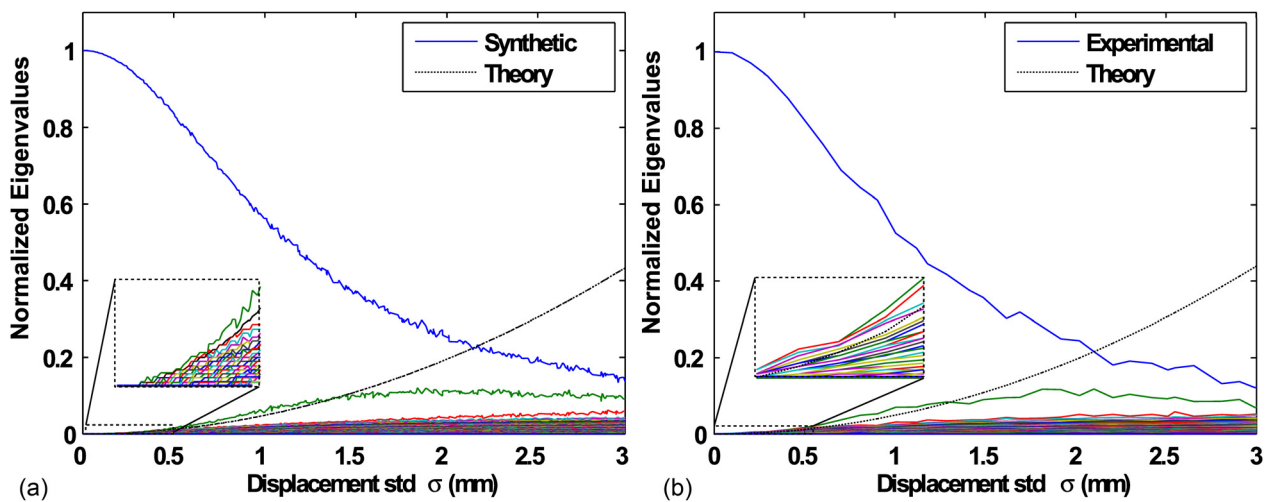

FIG. 10. (Color online) Element by element acquisition. Comparison of the eigenvalues of $\mathbf{K}^\dagger\mathbf{K}$ computed from synthetic (a) and experimental (b) MDM (solid lines) as a function of the standard deviation of the displacement. These curves are compared to Eq. (21) (dotted line). The configuration is the same as that in Fig. 3 except for $L = 175$ mm.
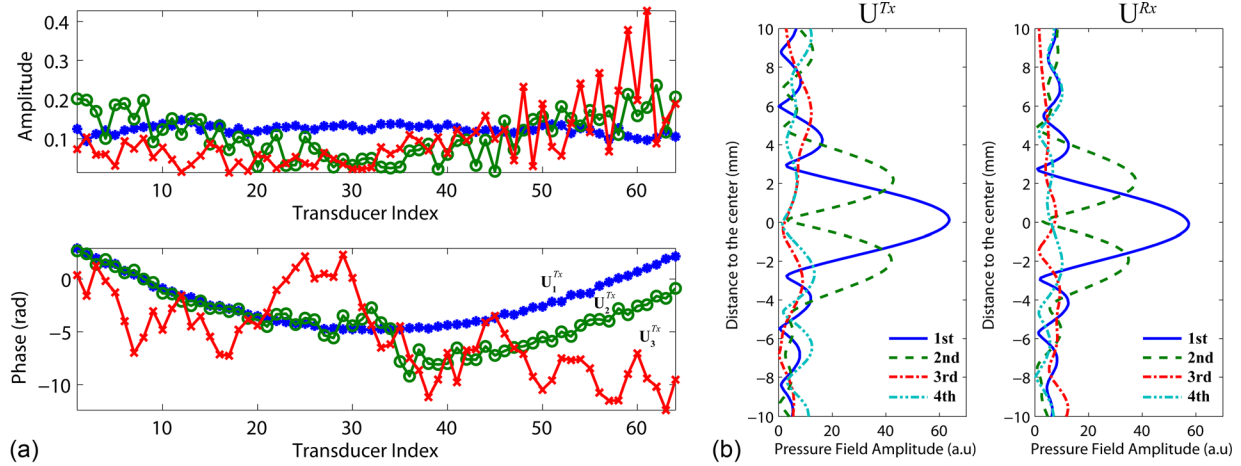
FIG. 11. (Color online) Experimental element by element eigenvectors when $\sigma = 0.70\,\text{mm}$. (a) Amplitude and phase of the three first experimental eigenvectors $\mathbf{U}_1^{Tx}(*)$, $\mathbf{U}_2^{Tx}(\circ)$, and $\mathbf{U}_3^{Tx}(\times)$. (b) Beamforming of the first five Tx and Rx eigenvectors at a distance L of 175 mm. The first eigenvector shows a monopolar focusing while the second eigenvector shows a dipolar focusing. We have shown that the first two eigenvalues were dominated for $\sigma = 0.70\,\text{mm}$ by the mean value $\langle \mathbf{K} \rangle$.

acquisition, the spot width dramatically increases in the case of ML and MUSIC estimators. This sensitivity to target motion is due to the non-linear behavior of the ML and MUSIC algorithms.

In the case of the MUSIC estimator, the spot width is proportional the square root of $N - |\sum_{l=1}^{N} \exp(+ik\sqrt{L^2 + z_l^2})[\mathbf{U}_1^{Tx}]_l|^2$. In other words, the width depends on $1 - |\alpha|^2$ where α is the projection of the first eigenvector on the first vector of the basis resulting from Gram-Schmidt orthonormalization. Without motion, the eigenvector is equal to $\exp(-ikM_lP)/\sqrt{N}$, i.e., $|\alpha|^2 = 1$ and the spot width decays toward 0. With motion, the first eigenvector is decomposed over all the vectors of the aforementioned orthonormal basis. Because the eigenvector is normalized, $|\alpha|^2$ is now smaller than 1 and the width of the MUSIC spot becomes finite. Exact expressions of the singular vectors can be derived thanks to the same Taylor's expansion of the time-reversal operator than the one performed in order to work out analytical expressions of the eigenvalues. The complete derivation of the vector is quite technical and out of the scope of this paper. Here, we only give the main results. The factors $1 - |\alpha|^2$ are equal to $a^4\sigma^4k^4/720L^4$ and $a^2\sigma^2k^2/12L^2$ for the Rx and Tx column by column acquisition, respectively. This result explains why the MUSIC spot is smaller for the estimator computed with Rx eigenvectors [Fig. 12(b)] than the one computed with Tx eigenvectors (here $a\sigma k/L < 1$) [Fig. 12(c)]. As for the element by element acquisition, because the matrix is statistically symmetric, the Tx and Rx spots are almost identical [Figs. 12(d) and 12(e)]. In that case, one can show that the factor $1 - |\alpha|^2$ is equal to $a^2\sigma^2k^2/6NL^2$. Applied to the parameters used to obtain the synthetic results shown in Fig. 12, the last factor, i.e., the spot width, is between the two previous ones.

The ML results are more complex to analyze. We have seen that for the element by element acquisition, the first eigenvalue is much larger than the other ones. In such a case the ML estimator is close to the MUSIC one: The two estimators provide similar spots. It is different for the column by col-

umn acquisition where the ML spot using Rx eigenvectors seems worse than the one using Tx eigenvectors. This effect may be explained by the fact that the Rx eigenvectors are expressed in terms of the target positions (see Sec. III) while on the contrary, it can be shown that the Tx eigenvectors mainly depend on the transducers positions and the average properties of the target displacement. Consequently, the maximum of the ML processing is less sensitive to target displacement when using Tx eigenvectors.
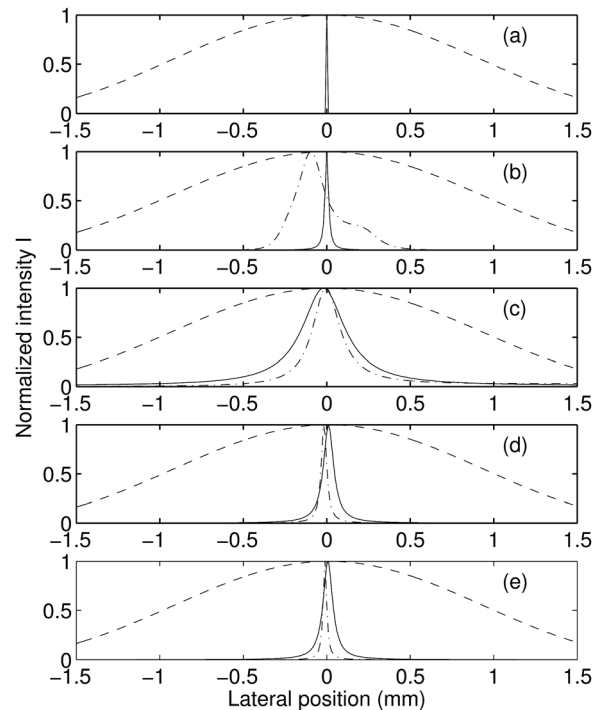

FIG. 12. Lateral target detection at range $L = 136\,\text{mm}$ from synthetic data using beamforming (dashed line), MUSIC (continuous line), and ML (dashed–dotted line) estimators. A $-60\,\text{dB}$ level noise is added. The noise is Gaussian distributed and decorrelated between all the array transducers. (a) is obtained for a motionless target. (b) and (c) [respectively, (d) and (e)] are worked out from a column by column (respectively, element by element) acquisition of the MDM for a target that moves randomly ($\sigma = 0.2\,\text{mm}$). (b) and (d) [respectively, (c) and (e)] are computed from Rx (respectively, Tx) invariants.

VI. CONCLUSION

We have presented a theoretical and experimental study of the eigenvalues of the TRO for a moving target. We have shown that target motion increases the rank of the MDM leading to supplementary "time reversal invariants." For detection purposes, this effect may induce false positive alerts. In the case of column by column acquisition, the eigenvalues increase as a power law of the displacement while for element by element acquisition of the MDM, two phenomena are observed: One is due to the fluctuations of the MDM and the other is related to the mean value. The random part of the MDM induces an eigenvalue continuum that grows linearly with respect to σ^2 whereas for the mean part, the eigenvalues follow a power law. Analytical formulations of the evolution of the eigenvalues have been given for both acquisition methods and confirmed by synthetic data or ultrasonic water tank experiments. A thorough study of eigenvalues and eigenvectors provides the target displacement. To finish, we have quantified the effect of such uncontrolled target displacements on two non-linear detection array processing. The degradation of the target localization strongly depends on the MDM acquisition method and on the applied detection algorithm.

APPENDIX A: EXPRESSION OF THE VECTORS $\tilde{\mathbf{V}}_m$

We use the Gram-Schmidt orthonormalization method on the family of vectors $\{[Z^{(m)}]^n, n \in \mathbb{N}\}$ to construct the new basis $\{\tilde{\mathbf{V}}_m, m \in \mathbb{N}\}$. The mth vector is proportional to the perpendicular component of $[(Z^{(1)})^m, (Z^{(2)})^m, \ldots, (Z^{(N)})^m]$ to $\tilde{\mathbf{V}}_1, \tilde{\mathbf{V}}_2, \ldots, \tilde{\mathbf{V}}_{n-1}$. In other words

$$(\tilde{\mathbf{V}}_m)_l = \frac{\left(Z^{(l)}\right)^m - \left[\sum_k (\tilde{\mathbf{V}}_{m-1})_k \left(Z^{(k)}\right)^m\right](\tilde{\mathbf{V}}_{m-1})_l - \ldots - \left[\sum_k (\tilde{\mathbf{V}}_0)_k \left(Z^{(k)}\right)^m\right](\tilde{\mathbf{V}}_0)_l}{\left\|\left(Z^{(l)}\right)^m - \left[\sum_k (\tilde{\mathbf{V}}_{m-1})_k \left(Z^{(k)}\right)^m\right](\tilde{\mathbf{V}}_{m-1})_l - \ldots - \left[\sum_k (\tilde{\mathbf{V}}_0)_k \left(Z^{(k)}\right)^m\right](\tilde{\mathbf{V}}_0)_l\right\|}. \tag{A1}$$

For example

$$(\tilde{\mathbf{V}}_0)_l = \frac{1}{\sqrt{N}},$$

$$(\tilde{\mathbf{V}}_1)_l = \frac{Z^{(l)}\left[\sum_k \frac{Z^{(k)}}{\sqrt{N}}\right]\frac{1}{\sqrt{N}}}{\left\|Z^{(l)} - \sum_k \frac{Z^{(k)}}{N}\right\|} = \frac{Z^{(l)}}{\sqrt{N}},$$

$$(\tilde{\mathbf{V}}_2)_l = \frac{\left(Z^{(l)}\right)^2\left[\sum_k \frac{(Z^{(k)})^3}{\sqrt{N}}\right]\frac{Z^{(l)}}{\sqrt{N}} - \left[\sum_k \frac{(Z^{(k)})^2}{\sqrt{N}}\right]\frac{1}{\sqrt{N}}}{\left\|\left(Z^{(l)}\right)^2 - \left[\sum_k \frac{(Z^{(k)})^3}{N}\right]\frac{Z^{(l)}}{\sqrt{N}} - \left[\sum_k \frac{(Z^{(k)})^2}{N}\right]\frac{1}{\sqrt{N}}\right\|} = \frac{\left(Z^{(l)}\right)^2 - 1}{\sqrt{2N}}. \tag{A2}$$

The right-hand side expressions in Eq. (A2) requires symmetrical displacement. In the case of symmetrical random displacement, the law of large numbers is also mandatory.

APPENDIX B: THE SECOND ORDER TAYLOR EXPANSION OF $\hat{\mathbf{H}}$

We start from Eq. (5)

$$(\tilde{H})_{ml} = (\tilde{K}^\dagger \tilde{K})_{ml}$$
$$= \frac{1}{(4\pi L)^4}\frac{N}{d}\int_{-d/2}^{d/2} e^{ik\left[\sqrt{L^2+(z-\sigma Z^{(m)})^2}-\sqrt{L^2+(z-\sigma Z^{(l)})^2}\right]} dz, \tag{B1}$$

where N is the number of elements in the array, L is the distance between the array and the target, d is the array length, z denotes the positions of the array elements, and $\sigma Z^{(l)}$ $(1 \leq l \leq N)$ the positions of the target during acquisition l.

The second order Taylor series expansion of $\tilde{\mathbf{H}}$ around $\sigma = 0$ is written as

$$(\tilde{K}^\dagger \tilde{K})_{ml} = \frac{N}{(4\pi L)^4}\left[1 - \sigma^2\left(c_1(Z^{(m)} - Z^{(l)})^2 + ic_2[(Z^{(m)})^2 - (Z^{(l)})^2]\right)\right] + o(\sigma^4), \tag{B2}$$

with

$$c_1 = \frac{k^2}{2d}\int_{-d/2}^{d/2}\frac{x^2}{x^2+L^2}dx = \frac{k^2}{2}\left(1 - \frac{2L}{d}\arctan\left(\frac{d}{2L}\right)\right),$$

$$c_2 = \frac{k}{2d}\int_{-d/2}^{d/2}\frac{L}{x^2+L^2}dx = \frac{k}{d}\arctan\left(\frac{d}{2L}\right). \tag{B3}$$

Philippe *et al.*: Time reversal and moving target

Assuming $d \ll 2L$, c_1 can be approximated by

$$c_1 \simeq \frac{k^2 d^2}{24L^2}.$$

The imaginary term in Eq. (B2) can be neglected as it will only add a phase term to the eigenvectors and will not change the eigenvalues of $\tilde{\mathbf{H}}$. The computation of the elements of $\hat{\mathbf{H}}$ is carried out as follows:

$$\hat{H}_{(m+1)(m'+1)} = \tilde{\mathbf{V}}_m^\dagger \tilde{\mathbf{H}} \tilde{\mathbf{V}}_{m'} = N \sum_{l=1}^{N} \sum_{l'=1}^{N} (\tilde{V}_m)_l$$
$$\times [1 - \sigma^2 c_1 (Z^{(l)} - Z^{(l')})^2](\tilde{V}_m)_{l'}. \quad \text{(B4)}$$

For instance, for $m = 1$ and $m' = 3$

$$\hat{H}_{13} = N \sum_{l=1}^{N} \sum_{l'=1}^{N} \frac{1}{\sqrt{N}}$$
$$\times [1 - \sigma^2 c_1 (Z^{(l)} - Z^{(l')})^2] \frac{(Z^{(l')})^2 - 1}{\sqrt{2N}}. \quad \text{(B5)}$$

Thanks to the orthogonality between $\tilde{\mathbf{V}}_0$ and $\tilde{\mathbf{V}}_2$, the previous expression becomes

$$\hat{H}_{13} \simeq -N\sigma^2 \frac{k^2 d^2}{24L^2} \sum_{l=1}^{N} \sum_{l'=1}^{N} (Z^{(l)} - Z^{(l')})^2 \frac{(Z^{(l')})^2 - 1}{N\sqrt{2}}$$

$$\simeq -N\sigma^2 \frac{k^2 d^2}{24L^2} \left[\sum_{l=1}^{N} \sum_{l'=1}^{N} (Z^{(l)})^2 \frac{(Z^{(l')})^2 - 1}{N\sqrt{2}} - 2 \sum_{l=1}^{N} \sum_{l'=1}^{N} (z^{(l)} z^{(l')}) \frac{(Z^{(l')})^2 - 1}{N\sqrt{2}} + \sum_{l=1}^{N} \sum_{l'=1}^{N} (Z^{(l')})^2 \frac{(Z^{(l')})^2 - 1}{N\sqrt{2}} \right]. \quad \text{(B6)}$$

To simplify the expression, we assume that all $Z^{(1)}$ are uncorrelated random Gaussian variables. The previous equation can be reduced to its third term. Indeed the odd moments of $Z^{(l)}$ are null, and the variance of $Z^{(l)}$ is equal to 1. Finally, Eq. (B6) is simplified to

$$\hat{H}_{13} \simeq -N\sigma^2 \frac{k^2 d^2}{24L^2} \sum_{l=1}^{N} \sum_{l'=1}^{N} \frac{(Z^{(l')})^4 - (Z^{(l')})^2}{N\sqrt{2}} \simeq -N^2 \sigma^2 \frac{k^2 d^2}{24L^2} \sum_{l'=1}^{N} \frac{(Z^{(l')})^4 - (Z^{(l')})^2}{N\sqrt{2}}$$

$$= -N^2 \sigma^2 \frac{k^2 d^2}{24L^2} \frac{3N - N}{N\sqrt{2}} \simeq -\frac{\sqrt{2} N^2 \sigma^2 k^2 d^2}{24L^2}. \quad \text{(B7)}$$

In Eq. (B7), the law of large numbers is used to replace the sum over l' by the mean value times N.

APPENDIX C: SYMETRIC DISPLACEMENT DISTRIBUTION

In this appendix, we show that when the parities of m and m' are different, the elements $\hat{H}_{mm'}$ equal zero.

The element $\hat{H}_{(m+1)(m'+1)}$ is equal to $\tilde{\mathbf{V}}_m^\dagger \tilde{\mathbf{H}} \tilde{\mathbf{V}}_{m'}$. This expression is a sum of the terms $\kappa_{p,p'} = \sum_{l,l'}^{N,N} (Z^{(l)})^p F(\sigma Z^{(l)}, \sigma Z^{(l')})(Z^{(l')})^{p'}$. A symmetric displacement distribution means that for each scatterer position $Z^{(l)}$, a symmetric one $Z^{(l')}$ exists, such that $Z^{(l')} = -Z^{(l)}$. Consequently

$$\kappa_{p,p'} = \sum_{l,l'}^{N,N} (Z^{(l)})^p F(\sigma Z^{(l)}, \sigma Z^{(l')})(Z^{(l')})^{p'} = \sum_{l+,l+'}^{N/2,/N/2} (Z^{(l)})^p F(\sigma Z^{(l+)}, \sigma Z^{(1+')})(Z^{(l+')})^{p'}$$

$$+ \sum_{l+,l+'}^{N/2,/N/2} (-Z^{(l+)})^p F(-\sigma Z^{(l+)}, \sigma Z^{(l+')})(Z^{(l+')})^{p'} + \sum_{l+,l+'}^{N/2,/N/2} (Z^{(l+)})^p F(\sigma Z^{(l+)}, -\sigma Z^{(l+')})(-Z^{(l+')})^{p'}$$

$$+ \sum_{l+,l+'}^{N/2,/N/2} (-Z^{(l+)})^p F(-\sigma Z^{(l+)}, -\sigma Z^{(l+')})(-Z^{(l+')})^{p'}, \quad \text{(C1)}$$

where the $l+$ and $l+'$ indices only refer to the positive scatterer positions. The function F is symmetric with respect to its two entries, i.e., $F(\sigma Z^{(l+)}, \sigma Z^{(l+')}) = F(-\sigma Z^{(l+)}, -\sigma Z^{(l+')})$.

The previous equation can be rewritten as

$$\sum_{l,m}^{N,N} \left(Z^{(l)}\right)^p F(\sigma Z^{(l)}, \sigma Z^{(m)}) \left(Z^{(m)}\right)^{p'} = \sum_{l+,l+'}^{N/2,/N/2} \left(Z^{(l)}\right)^p F(\sigma Z^{(l)}, \sigma Z^{(l+')}) \left(Z^{(l+')}\right)^{p'} [1 + (-1)^{p+p'}]$$
$$+ \sum_{l+,l+'}^{N/2,/N/2} \left(Z^{(l+)}\right)^p F(-\sigma Z^{(l+)}, \sigma Z^{(1+')}) \left(Z^{(l+')}\right)^{p'} [(-1)^p + (-1)^{p'}]. \tag{C2}$$

It is now clear that when the parities of p and p' are different, the expression is equal to zero. Due to the Gram-Schmidt orthonormalization method, the lth element of vector $\mathbf{V}_p$ is a polynomial sum of terms $Z^{(l)}$ (see Appendix A). For symmetrical displacements, all the power exponents involved in the sum have the same parity than p (if p is odd, all the power exponents are odd and vice-versa). Consequently, $\sum_{l,m}^{N,N} (V_p)_l F(\sigma Z^{(l)}, \sigma Z^{(m)})(V_{p'})_m = 0$, i.e., $\tilde{\mathbf{V}}_m^{\dagger} \tilde{\mathbf{H}} \tilde{\mathbf{V}}_{m'} = 0$, when the parities of p and p' are different. Because of the law of large numbers, this property still holds for random symmetrical displacements when $N \gg 1$.

APPENDIX D: EXPRESSION OF THE ELEMENTS OF $\hat{\mathbf{H}}$

Using the method described in Appendix B, the dominant terms of the non-zero elements of the matrix $\hat{\mathbf{H}}$ are written ($\hat{\mathbf{H}}$ is symmetric) as

$$\hat{H}_{11} \simeq N^2 - \frac{d^2 N^2 k^2 \sigma^2}{12L^2},$$
$$\hat{H}_{13} \simeq -\frac{\sqrt{2} N^2 k^2 \sigma^2}{24L^2},$$
$$\hat{H}_{22} \simeq \frac{d^2 N^2 k^2 \sigma^4}{12L^2},$$
$$\hat{H}_{15} \simeq \frac{\sqrt{6} N^2 k^2 \sigma^4}{4L^2}, \tag{D1}$$
$$\hat{H}_{42} \simeq \frac{\sqrt{6} d^4 N^2 k^4 \sigma^4}{480L^4},$$
$$\hat{H}_{33} \simeq \frac{N^2 k^2 \sigma^4}{2L^2}.$$

APPENDIX E: DERIVATION TO THE SECOND TAYLOR ORDER

Up to the second Taylor order of the derivation the displacement the matrix $\hat{\mathbf{H}}$ is written as

$$\begin{bmatrix} N^2 - \dfrac{d^2 N^2 k^2 \sigma^2}{12L^2} & 0 & -\dfrac{\sqrt{2} d^2 N^2 k^2 \sigma^2}{24L^2} \\[3mm] 0 & \dfrac{d^2 N^2 k^2 \sigma^2}{12L^2} & 0 \\[3mm] -\dfrac{\sqrt{2} d^2 N^2 k^2 \sigma^2}{24L^2} & 0 & 0 \end{bmatrix}. \tag{E1}$$

This matrix has obviously a second eigenvalue equal to $d^2 N^2 k^2 \sigma^2 / 12L^2$ associated with the eigenvector $\tilde{\mathbf{V}}_1$. The other eigenvalues are derived by calculating the determinant of the remaining matrix

$$\begin{vmatrix} N^2 - \dfrac{d^2 N^2 k^2 \sigma^2}{12L^2} - \Sigma & -\dfrac{\sqrt{2} d^2 N^2 k^2 \sigma^2}{24L^2} \\[3mm] -\dfrac{\sqrt{2} d^2 N^2 k^2 \sigma^2}{24L^2} & -\Sigma \end{vmatrix}$$
$$= \left(-N^2 + \dfrac{d^2 N^2 k^2 \sigma^2}{12L^2} + \Sigma\right) \Sigma + O(\sigma^4). \tag{E2}$$

The roots of the determinant give the first and third eigenvalues $\Sigma_1 = N^2 - d^2 N^2 k^2 \sigma^2 / 12L^2 + O(\sigma^4)$ and $\Sigma_3 = 0 + O(\sigma^4)$. Thus the leading term of the third eigenvalue is at least of fourth Taylor order.

Note that the Gaussian assumption and the law of large numbers are only required for the off diagonal matrix elements. Because these terms only contribute at Taylor order 4, up to Taylor order 2, the two first eigenvalue expressions are also valid for non-Gaussian motions (e.g., a deterministic motion).

[1]N. Chakroun, M. Fink, and F. Wu, "Time reversal processing in ultrasonic nondestructive testing," IEEE Trans. Ultrason. Ferroelect. Freq. Contr. **42**(6), 1087–1098 (1995).

[2]V. Miette, L. Sandrin, F. Wu, and M. Fink, "Optimisation of time reversal processing in titanium inspections," Proc.-IEEE Ultrason. Symp. **1**, 643–647 (1996).

[3]J.-L. Thomas and M. A. Fink, "Ultrasonic beam focusing through tissue inhomogeneities with a time reversal mirror: Application to transskull therapy," IEEE Trans. Ultrason. Ferroelect. Freq. Contr. **43**(6), 1122–1129 (1996).

[4]M. Pernot, J. F. Aubry, M. Tanter, A. L. Boch, F. Marquet, M. Kujas, D. Seilhean, and M. Fink, "In-vivo transcranial brain surgery with an ultrasonic time reversal mirror," J. Neurosurg. **106**, 1061–1066 (2007).

[5]J.-L. Thomas, F. Wu, and M. Fink, "Time reversal focusing applied to lithotripsy," Ultrason. Imaging **18**, 106–121 (1996).

[6]W. A. Kuperman, W. S. Hodgkiss, H. C. Song, T. Akal, C. Ferla, and D. R. Jackson, "Phase conjugation in the ocean: Experimental demonstration of an acoustic time-reversal mirror," J. Acoust. Soc. Am. **103**, 25–40 (1998).

[7]W. S. Hodgkiss, H. C. Song, W. A. Kuperman, T. Akal, C. Ferla, and D. R. Jackson, "A long-range and variable focus phase conjugation experiment in shallow water," J. Acoust. Soc. Am. **105** 1597–1604 (1998).

[8]T. Shimura, H. Ochi, and Y. Watanabe, "First experiment result of time-reversal communication in deep ocean," Jpn. J. Appl. Phys. **46**, 7b (2007).

[9]A. Silva, S. Jesus, J. Gomes, and V. Barroso. "Underwater acoustic communications using a 'virtual' electronic time-reversal mirror approach," in *5th European Conference on Underwater Acoustics*, edited by P. Chevret and M. Zakharia (Lyon, France, 2000), pp. 531–536.

[10]D. R. Dowling, "Phase conjugate array focusing in a moving medium," J. Acoust. Soc. Am. **94**(3), 1716–1718 (1993).

[11]P. Roux and M. Fink, "Time reversal in a waveguide: Study of the temporal and spatial focusing," J. Acoust. Soc. Am. **107**(5), 2418–2429 (2000).

[12]K. G. Sabra and D. R. Dowling, "Effects of time-reversing array deformation in an ocean wave guide," J. Acoust. Soc. Am. **115**, 2844–2847 (2004).

[13]C. Prada, F. Wu, and M. Fink, "The iterative time reversal mirror: A solution to self-focusing in the pulse echo mode," J. Acoust. Soc. Am. **90**, 1119–1129 (1991).

[14]C. Prada, J. de Rosny, D. Clorennec, J.-G. Minonzio, A. Aubry, M. Fink, L. Berniere, P. Billand, S. Hibral, and T. Folegot. "Experimental detection and focusing in shallow water by decomposition of the time reversal operator," J. Acoust. Soc. Am. **122**, 761–768 (2007).

[15]N. Mordant, C. Prada, and M. Fink, "Highly resolved detection and selective focusing in a waveguide using the D.O.R.T. method," J. Acoust. Soc. Am. **105**, 2634–2642 (1999).

[16]F. D. Philippe, C. Prada, J. de Rosny, D. Clorennec, J.-G. Minonzio, and M. Fink, "Characterization of an elastic target in a shallow water waveguide by decomposition of the time-reversal operator," J. Acoust. Soc. Am. **124**(2), 779–787 (2008).

[17]The Green's function G(A,B) between positions A and B is equal to $\exp(ikR_{AB})/4\pi R_{AB}$ where R_{AB} is the distance between points A and B.

[18]G. Barton, *Elements of Green's Functions and Propagation: Potentials, Diffusion, and Waves* (Clarendon Press/Oxford University Press, Oxford/New York, 1989), Chap. 12, pp. 339–344.

[19]H. Bucker, "Matched-field tracking in shallow water," J. Acoust. Soc. Am. **96**, 3809–3811 (1994).

[20]M. J. Wilmut and J. M. Ozard, "Detection performance of two efficient source tracking algorithms for matched-field processing," J. Acoust. Soc. Am. **104**, 3351–3355 (1998).

[21]S. L. Tantum and L. W. Nolte, "Tracking and localizing a moving source in an uncertain shallow water environment," J. Acoust. Soc. Am. **103**, 362–373 (1998).

[22]J. Baik and J. Silverstein, "Eigenvalues of large sample covariance matrices of spiked population models," J. Multivariate Anal. **97**, 1382–1408 (2006).

[23]M. Capitaine, C. Donati-Martin, and D. Féral, "The largest eigenvalue of finite rank deformation of large Wigner matrices: Convergence and nonuniversality of the fluctuations," Ann. Probab. **37**, 1–47 (2009).

[24]H. Ammari, J. Garnier, H. Kang, W. K. Park, and K. Sølna, "Imaging schemes for cracks and inclusions," SIAM J. Appl. Math. **71**, 68–91 (2011).

[25]M. L. Mehta, "Random matrices," in *Pure and Applied Mathematics* (Elsevier, San Diego, 2004), Vol. 142, Chap. 4.2, pp. 65–67.

[26]The maximum singular value of a matrix with independent complex Gaussian entries of variance $1/N$ when N approaches infinity is equal to 2.

[27]C. Prada and J.-L. Thomas, "Experimental sub-wavelength localization of scatterers by decomposition of the time reversal operator interpreted as a covariance matrix," J. Acoust. Soc. Am. **114**, 235–243 (2003).